Atmos. Chem. Phys., 11, 12369–12386, 2011
www.atmos-chem-phys.net/11/12369/2011/
doi:10.5194/acp-11-12369-2011

Atmospheric Chemistry and Physics

Aerosol hygroscopicity and CCN activation kinetics in a boreal forest environment during the 2007 EUCAARI campaign

K. M. Cerully[1], T. Raatikainen[2,3], S. Lance[4,5], D. Tkacik[6], P. Tiitta[7,8], T. Petäjä[9], M. Ehn[9,*], M. Kulmala[9], D. R. Worsnop[3,7,9,10], A. Laaksonen[3,7], J. N. Smith[7,11], and A. Nenes[1,2,12]

[1]School of Chemical and Biomolecular Engineering, Georgia Institute of Technology, Atlanta, GA, USA
[2]School of Earth and Atmospheric Science, Georgia Institute of Technology, Atlanta, GA, USA
[3]Finnish Meteorological Institute, Helsinki, Finland
[4]Cooperative Institute for Research in Environmental Sciences, University of Colorado, Boulder, CO, USA
[5]Earth System Research Laboratory, National Oceanic and Atmospheric Administration, Boulder, CO, USA
[6]Center for Atmospheric Particle Studies, Carnegie Mellon University, Pittsburgh, PA, USA
[7]Department of Applied Physics, University of Eastern Finland, Kuopio, Finland
[8]Atmospheric Chemistry Research Group, North-West University, Potchefstroom, South Africa
[9]Department of Physics, University of Helsinki, Helsinki, Finland
[10]Aerodyne Research Incorporated, Billerica, MA, USA
[11]National Center for Atmospheric Research, Boulder, CO, USA
[12]Institute of Chemical Engineering and High-Temperature Chemical Processes, Foundation for Research and Technology Hellas, Patras, Greece
[*]currently at: Institute for Energy and Climate Research, Forschungszentrum Jülich, Jülich, Germany

Received: 20 April 2011 – Published in Atmos. Chem. Phys. Discuss.: 18 May 2011
Revised: 1 November 2011 – Accepted: 9 November 2011 – Published: 9 December 2011

Abstract. Measurements of size-resolved cloud condensation nuclei (CCN) concentrations, subsaturated hygroscopic growth, size distribution, and chemical composition were collected from March through May, 2007, in the remote Boreal forests of Hyytiälä, Finland, as part of the European Integrated project on Aerosol Cloud Climate and Air Quality Interactions (EUCAARI) campaign. Hygroscopicity parameter, κ, distributions were derived independently from Continuous Flow-Streamwise Thermal Gradient CCN Chamber (CFSTGC) and Hygroscopicity Tandem Differential Mobility Analyzer (HTDMA) measurements. CFSTGC-derived κ values for 40, 60, and 80 nm particles range mostly between 0.10 and 0.40 with an average characteristic of highly oxidized organics of 0.20 ± 0.10, indicating that organics play a dominant role for this environment. HTDMA-derived κ were generally 30 % lower. Diurnal trends of κ show a minimum at sunrise and a maximum in the late afternoon; this trend covaries with inorganic mass fraction and the *m/z* 44 organic mass fraction given by a quadrupole aerosol mass spectrometer, further illustrating the importance of organics in aerosol hygroscopicity. The chemical dispersion inferred from the observed κ distributions indicates that while 60 and 80 nm dispersion increases around midday, 40 nm dispersion remains constant. Additionally, 80 nm particles show a markedly higher level of chemical dispersion than both 40 and 60 nm particles. An analysis of droplet activation kinetics for the sizes considered indicates that most of the CCN activate as rapidly as $(NH_4)_2SO_4$ calibration aerosol.

Correspondence to: A. Nenes
(athanasios.nenes@gatech.edu)

1 Introduction

Atmospheric aerosols are known to have a direct effect on climate through scattering and absorbing incoming solar radiation (IPCC, 2007). They also indirectly affect climate by acting as cloud condensation nuclei (CCN), and modifying cloud forcing and the hydrological cycle (Twomey, 1974, 1977). While it is generally thought that aerosols produce an overall cooling effect, the indirect effect remains a large source of uncertainty in predictions of anthropogenic climate change (e.g., IPCC, 2007). For this reason, the study of aerosol and their CCN properties is necessary for an improved understanding of aerosol-cloud-climate interactions.

The ability of an aerosol particle to act as CCN depends on both its size and composition (Köhler, 1936; Seinfeld and Pandis, 2006). Köhler theory uses thermodynamic arguments to describe how changes in curvature (known as the Kelvin effect) and the amount of solute (known as the Raoult effect) impact the equilibrium vapor pressure of a droplet. Using this theory, the critical supersaturation, above which an aerosol particle "activates" spontaneously into a cloud droplet, can be predicted. While originally developed for inorganic salts, Köhler theory can be extended to include effects of organics through their contribution of solute and surface tension depression (e.g., Shulman et al., 1996; Li et al., 1998; Raymond and Pandis, 2002). κ-Köhler theory (Petters and Kreidenweis, 2007) parameterizes solute contribution in terms of a single hygroscopicity parameter, κ, and represents a "scaled" volume fraction of soluble material in the particle (Lance, 2007; Padró et al., 2010). Typical soluble salts found in the atmosphere such as ammonium sulfate or sodium chloride have values of $\kappa \approx 0.6$ and $\kappa \approx 1.2$, respectively (Petters and Kreidenweis, 2007), while $\kappa = 0$ corresponds to a completely insoluble particle. Lab and field studies show that κ of secondary organic aerosol (SOA) typically ranges between 0.1 and 0.2 (e.g., Prenni et al., 2007; Gunthe et al., 2009; Dusek et al., 2010; Engelhart et al., 2008, 2011; Asa-Awuku et al., 2009, Sihto et al., 2010), although the water-soluble fraction extracted from a range of SOA systems and biomass burning exhibits $\kappa \approx 0.3$ (Asa-Awuku et al., 2010; Padró et al., 2010; Engelhart et al., 2008, 2011). For many locations, on average, κ values for continental and marine aerosols have been typically found to be 0.3 ± 0.2 and 0.7 ± 0.2, respectively (e.g., Andreae and Rosenfeld, 2008; Pringle et al., 2010); however, assuming a constant κ can introduce a sizeable uncertainty in CCN number predictions (e.g., Chang et al., 2010; Pöschl, 2011).

Size-resolved CCN measurements offer unique insight on compositional dispersion and the processes that affect aerosol hygroscopicity (e.g., Lance, 2007; Padró et al., 2007, 2010; Gunthe et al., 2009; Petters et al., 2009; Rose et al., 2010; Asa-Awuku et al., 2009, 2010; Mochida et al., 2010; Irwin et al., 2011; Bougiatioti et al., 2011). Petters et al. (2009) found that κ from emissions of fresh biomass burning generally decreased with particle size, although varying κ distributions and several hygroscopic modes may occur. During the AMAZE-08 Campaign at a remote site in Brazil, Aitken mode particles ($\sim$50 nm) had κ of 0.1, characteristic of the hygroscopicity of biogenic SOA, while accumulation mode ($\sim$200 nm) particles had an increased κ of 0.2, correlating with a 10 % increase in sulfate (Gunthe et al, 2009; Pöschl et al., 2010). In Finokalia, Crete, however, Bougiatioti et al. (2011) found that smaller particles (40 nm) generally had κ about 0.1 units greater than that of larger particles (100 nm). While the previous studies showed strongly size-dependent hygroscopicity, Mochida et al. (2010) found that, for 34 particle sizes ranging from 24.1 to 359 nm sampled in Cape Hedo, Okinawa, Japan, the particles typically showed unimodal, high hygroscopicity likely due to internally mixed particles rich in ammonium sulfate.

Bulk and size-resolved measurements of aerosol composition are important for further deconvolving the effects of composition on CCN properties and behavior. In a study of CCN closure, Lance et al. (2009) showed that average CCN overprediction bias during the GoMACCS field mission in Houston, Texas, was reduced from 36 % to 3 % when bulk aerosol chemical composition from an Aerosol Mass Spectrometer (AMS) was included. Bougiatioti et al. (2009, 2011) obtained underprediction bias as low as 0.6 ± 9 % when including bulk composition measurements from analysis of PTFE and quartz filter samples in the eastern Mediterranean during the FAME07 campaign. While certain conditions or environments allow for a reasonable comparison of bulk composition data with smaller aerosol particles, this may not always be the case. Medina et al. (2007) overpredicted CCN by 35.8 ± 28.5 % in a CCN closure study when using AMS size-averaged chemical composition, but only 17.4 ± 27.0 % when using size-dependent composition during the ICARTT 2004 campaign at a rural site in New Hampshire. Gunthe et al. (2009) also found for a pristine tropical rainforest environment that the high bias in predicted CCN to measured CCN was a result of using bulk rather than size-resolved AMS data. Beyond CCN closure, composition measurements are able to elucidate the physicochemical processes occurring in the atmosphere. For AMS measurements, in particular, while it is not possible to identify individual organic aerosol (OA) compounds from the measured mass spectra, a rough estimate of oxidation state can be derived from the mass fraction of the *m/z* 44 peak (CO_2^+) in the organic aerosol signal, f_{44}, originating mainly from decomposition of carboxyl groups during the ionization step in the AMS. f_{44} has been shown to correlate with *O/C* ratio in aerosol particles (Aiken et al., 2008) and the hygroscopicity of SOA-dominated aerosol (e.g., Jimenez et al., 2009; Raatikainen et al., 2010; Massoli et al., 2010). One can attribute the correlation between f_{44} and hygroscopicity to an increase of the water-soluble fraction of organic aerosol (Bougiatioti et al., 2009; Padró et al., 2010; Asa-Awuku et al., 2011).

Another uncertain aspect of cloud droplet formation is the impact of slowly-dissolving compounds, droplet surface films, and aerosol amorphous states on the activation kinetics of CCN. If present, kinetic inhibitions (beyond that expected from gas-to-particle mass transfer alone) could have an important impact on cloud droplet number and size distribution (e.g., Jensen and Charlson, 1984; Kulmala et al., 1993; Chuang et al., 1997; Nenes et al., 2001, 2002; Lance et al., 2004). Studies often detect the presence of CCN experiencing kinetic limitations by comparing the size of activated droplets against a standard of rapid activation (e.g., calibration salt CCN). Many studies have found little evidence of kinetic limitations (e.g., Chuang, 2003; Engelhart et al., 2008, 2011; Lance et al., 2009; Bougiatioti et al, 2009, 2011;

Asa-Awuku et al., 2010; Padró et al., 2010), although others detected kinetic limitations when the aerosol originated from above the boundary layer or contained a large fraction of hydrophobic organics (e.g., Sorooshian et al., 2008; Ruehl et al., 2008, 2009; Asa-Awuku et al., 2009, 2011). Padró et al. (2010) showed that the water-soluble organics in Mexico City during the MILAGRO campaign did not affect droplet growth rates. Asa-Awuku et al. (2009) showed that droplet growth kinetics were strongly anticorrelated with the water-soluble organic carbon fraction for β-caryophyllene SOA. Murphy et al. (2009) detected some kinetic limitations for organic-rich aerosol freshly emitted from a cargo ship. Lance et al. (2009) found that activation kinetics in the boundary layer were not greatly depressed over Houston, Texas, during the GoMACCS campaign, while Ruehl et al. (2008) and Asa-Awuku et al. (2011) found during the same campaign (but different location and time periods) that up to 30 % of the CCN may exhibit some degree of delayed condensational growth. Bougiatioti et al. (2009, 2011) found that aged carbonaceous aerosol sampled at a remote marine site in the eastern Mediterranean during the 2007 Finokalia Aerosol Measurement Experiment (FAME07) did not exhibit kinetically limited droplet growth rates. Ruehl et al. (2009) found strong kinetic limitations above the marine boundary layer near the California coast. These studies encompass a large range of environments and conditions; however the prevalence of kinetic limitations varies even for similar environments, suggesting the need for further investigation.

Boreal forests, such as the one considered in this study, offer a unique and climatically-important environment for study as they cover 8 % of the earth's surface (Sihto et al., 2010). Remote forests allow for looking at clean, "background" air masses with a strong dominance of biogenic SOA (Boy et al., 2004; Kulmala et al., 2004), illustrating the importance of interactions between the soil, ecosystem, and atmosphere (Hari and Kulmala, 2005; Barth et al., 2005; Kanakidou et al., 2005). The frequent occurrence of nucleation events in boreal forests influences the aerosol properties of different size modes (Hämeri et al., 2001). CCN studies for this type of environment have investigated the diurnal variation of critical activation diameter, hygroscopicity, solubility, and the properties of characteristic particle sizes and modes (e.g., Aalto and Kulmala, 2000; Hämeri et al., 2001; Sihto et al., 2010). It is expected that the influence of particle formation events and secondary organic aerosol (SOA) production give rise to CCN rich in carbonaceous material, but with a small fraction of inorganic salts that further augments their hygroscopicity (Sihto et al., 2010).

Size-resolved CCN concentrations, subsaturated hygroscopic growth, size distribution, and chemical composition were measured at Hyytiälä, Finland, during March through May, 2007, as part of the EUCAARI campaign (see Kulmala et al., 2009). The current study utilizes these measurements in order to investigate size-dependent hygroscopicity and CCN activation kinetics of aerosol in a boreal forest environment. An emphasis is placed on the diurnal variation of aerosol mixing state and composition and their effects on aerosol hygroscopicity.

2 Data Collection

2.1 Measurement Site

Data were collected from a comprehensive suite of aerosol instrumentation at the SMEAR II station (61°51′ N, 24°17′ E) located in a boreal forest in Hyytiälä, Finland, from 25 March through 15 May 2007. This site is described in detail in Kulmala et al. (2001) and Hari and Kulmala (2005). In addition to size-resolved CCN, subsaturated hygroscopic growth, size distribution, and chemical composition, measurements of temperature, wind direction, gas phase species concentrations, and particle size distributions were also collected. Hyytiälä receives air masses from a variety of sources and locations. The SMEAR II station sees both "clean" and "polluted" air masses which are often, but not always, characterized by low particle concentrations transported from the Arctic Ocean and northern Scandinavia and high particle concentrations transported from central and eastern Europe, respectively. An example of NOAA HYSPLIT backtrajectories (http://ready.arl.noaa.gov/HYSPLIT.php) characterizing clean and polluted air masses is shown in Fig. 1.

2.2 Instrument setup

A "stepping mode" setup for supersaturation and size (Lance, 2007; Moore et al., 2010) is used to obtain size-resolved CCN activity data. First, an ambient sample is introduced into a Differential Mobility Analyzer (DMA, TSI 3085). Dilution flow is then added to the classified aerosol stream before being split to a Condensation Particle Counter (CPC, TSI 3760A), giving the total number of particles or condensation nuclei (CN) and to a Continuous Flow-Streamwise Thermal Gradient CCN Chamber (CFSTGC) (Roberts and Nenes, 2005; Lance et al., 2006) manufactured by Droplet Measurement Technologies, Inc. While supersaturation is held constant in the CFSTGC, the mobility diameter in the DMA is stepped to obtain measurements of CCN and CN concentration at several particle sizes. For each particle size, the ratio of CCN to CN concentration, known as the "activation ratio", is computed. This procedure is then repeated for several other supersaturations to characterize the size-dependent CCN activity of particles.

During this study, the supersaturation, s, in the CFSTGC is held constant over a period of 3 min, during which particles sizes of 20, 40, 60, 80, and 100 nm were selected by the DMA (e.g, Fig. 2). Data collected up to 20 seconds after a change in DMA-selected particle size is discarded and the activation ratio is measured over a period of 16 s.

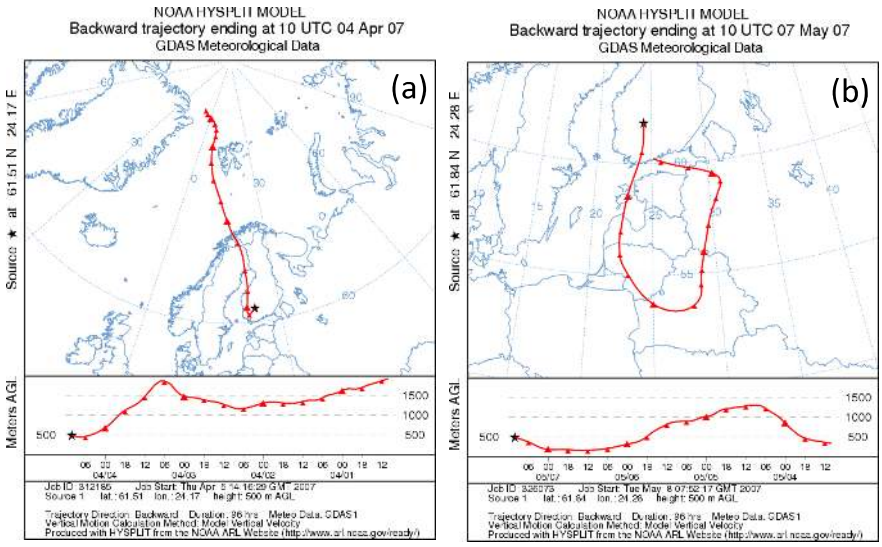

Fig. 1. HYSPLIT backtrajectories for **(a)** clean and **(b)** polluted air masses.

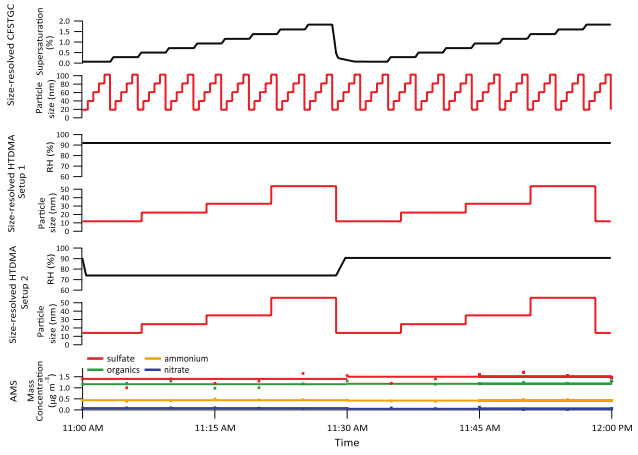

Fig. 2. Example of the operation schedule for CFSTGC, HTDMA, and AMS measurements. A schematic of the HTDMA measurement schedules for data collected up to 1 May and after 3 May are indicated as Setup 1 and Setup 2, respectively. An example of actual data collected by AMS is represented by circles, while lines represent 30 minute averages used for this study.

The 20 nm and 100 nm data were discarded, because activation spectra were not fully detected at the selected instrument supersaturation range and also as the instrument transients had an effect on the 20 nm data. Instrument supersaturation was stepped in increments of ∼0.2 % ranging from ∼0.1 % to 1.8 % for each particle size. An additional 3 min were allowed after switching from the highest to lowest supersaturation and data collected at the lowest supersaturation were discarded in order to allow sufficient time for the instrument supersaturation to reach the setpoint (e.g. Rose et al., 2008; Moore et al., 2010). This setup allowed for obtaining a cycle of size and supersaturation resolved CCN activity about every 30 min. The DMA was operated with a nominal aerosol flow rate of about 1 l min^{-1} and a sheath-to-aerosol flow rate ratio of ∼4.5:1. Dilution flow of 1 l min^{-1} was introduced directly following the DMA. The CPC required a flow rate of 1 l min^{-1}. The CFSTGC was operated at a total flow rate of 1 l min^{-1} with a sheath-to-aerosol flow rate ratio of ∼10:1. Supersaturation in the instrument was calibrated with laboratory-generated ammonium sulfate particles using the Scanning Mobility CCN Analysis (SMCA) method described by Moore et al. (2010).

The Hygroscopicity Tandem Differential Mobility Analyzer (HTDMA) measures the hygroscopic growth of size-classified particles exposed to a selected relative humidity (RH) below 100 % (e.g., Liu et al., 1978; Rader and McMurry, 1986; Swietlicki et al., 2008). The HTDMA used in the current study is fully described in Ehn et al. (2007), so only a brief description is given here. A first DMA unit is used to select a narrow size range from dried ambient particles. Then, the selected particles are exposed to a selected RH and the average growth of the humidified particles is measured by the second DMA unit and a CPC. A mean value representing average humid aerosol size is calculated from the humidified size distributions and is divided by the corresponding dry size to yield the hygroscopic growth factor (GF). The dry particle sizes of 10, 20, 30, and 50 nm, were selected by the first DMA in the HTDMA. These four particle sizes were stepped through over the course of approximately 30 min giving a single GF for each size every 30 min. Only the 30 and 50 nm data are shown for this study as they fall within the measured CCN data size range. For measurements collected up to 1 May, aerosol hygroscopic growth was

measured at 90 % RH. From 3 May through the end of the study, the RH was cycled between 71 % and 87 % each half hour (e.g., Fig. 2).

Aerosol chemical composition was measured by an Aerodyne AMS (e.g., Jayne et al., 2000; Allan et al., 2003, 2004; Jimenez et al., 2003; Alfarra et al., 2004; Canagaratna et al., 2007). Briefly, the instrument is capable of detecting mass concentrations of non-refractory species from sub-micron aerosol with a time resolution of about 10 min (Jimenez et al., 2003; Canagaratna et al., 2007). "Non-refractory" refers to species that volatilize rapidly at 600 °C, which means that crustal material, sea-salt, or black carbon aerosol cannot be detected. In practice, the AMS measures mass concentrations of non-sea-salt chloride, sulfate, nitrate, ammonium and organics ($\mu g\,m^{-3}$). Initially, the AMS was operated by altering between particle time of flight (pTOF) and mass spectrum (MS) modes (e.g., Jimenez et al., 2003), saving data every 10 min. On 4 April, the AMS was turned off and prepared for flux measurements (e.g., Nemitz et al., 2008). Starting from 6 April, the first 30 min of every hour was used for the flux measurements, and during the second 30 min period the AMS was alternating between pTOF, MS, and jump mass spectrum (JMS) modes (e.g., Crosier et al., 2007). In addition, averaging time was decreased to 5 minutes from the original value of 10 min. Mass concentrations were very noisy due to the short averaging time, so the AMS mass concentration (MS mode) data was averaged for each 30 min CCN measurement period (e.g., Fig. 2). The data coverage for the 30 min time base is 47 %. Most of the missing data points (42 % of all data points) are due to the flux measurements, but some data points (11 % of all data points) are missing due to routine maintenance and hardware failures.

3 Methodology

The CFSTGC and HTDMA provide hygroscopicity measurements under supersaturated and subsaturated conditions, respectively; each dataset can independently be used to derive κ distributions. Petters and Kreidenweis (2007) found that agreement between CCN-derived κ and HTDMA-derived κ is within 30 % for most compounds considered in their study. Slight differences may occur between subsaturated and supersaturated κ values, as droplet solutions of activated particles in the CFSTGC are typically more dilute than if measured at subsaturated conditions (e.g., Petters and Kreidenweis, 2007; Asa-Awuku et al., 2010). For κ obtained at subsaturated conditions, solution non-ideality, phase separation, and partial solubility of constituents may be more pronounced and affect (mostly decrease) the observed κ. Therefore, the HTDMA and CFSTGC provide two independent measures of hygroscopicity under very different water activity conditions; together, these measurements are often used to test and confirm the validity of experimental methods (e.g., Aalto and Kulmala, 2000; Good et al., 2010; Petters et al., 2009; Sihto et al., 2010; Irwin et al., 2011).

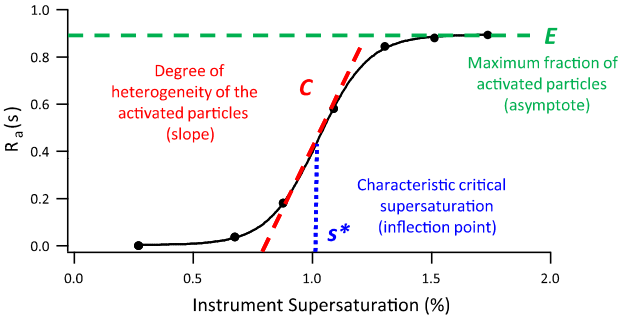

Fig. 3. Example of an activation spectra and fitted parameters.

From subsaturated HTDMA GF data for particles of dry diameter d_p, κ values were predicted using

$$\kappa = (\mathrm{GF}^3 - 1)\left(\frac{\exp(\frac{A}{\mathrm{GF}\,d_p})}{\frac{\mathrm{RH}}{100\,\%}} - 1\right) \quad (1)$$

where $A{=}(4M_w\sigma_w)/(RT\rho_w)$, M_w is the molar mass of water, σ_w is the surface tension of water, R is the universal gas constant, T is temperature, ρ_w is the density of water (Petters and Kreidenweis, 2007). Some GF values were removed from the analysis due to limited counting statistics at low particle concentrations based on an approximated background noise. The total percentage of GFs filtered from the analysis for the 30 and 50 nm datasets are ~14 % and 10 %, respectively. From the CCN data, the supersaturation-resolved activation ratio function, $R_a(s)$, for a given size particle is fit to a sigmoid with the form

$$R_a(s) = \frac{E}{1 + \left(\frac{s}{s^*}\right)^C} \quad (2)$$

where E is the maximum fraction of particles that activate at high supersaturations, s is the instrument supersaturation, s^* is the characteristic critical supersaturation of the CCN population, the supersaturation at which half of the ambient CCN activate (i.e. $R_a(s) = 0.5E$). C is a coefficient that is a measure of the slope of $R_a(s)$ and is affected by the chemical heterogeneity of the activated particles (Fig. 3).

Before fitting to Eq. (2), data were filtered for low CCN concentrations to avoid biases from insufficient counting statistics. This is done by applying Poisson statistics to describe the relative counting uncertainty as the inverse square root of the number concentration. Using the flow through the instrument during each 16 s measurement period, this number can be converted to a minimum acceptable concentration value. For the instrument setup used in this campaign, a relative uncertainty of 15 % resulted in a minimum detection limit of ~4 particles cm^{-3}, below which data were discarded. Equation (2) was then fit to a spectra of activated ratios at a

number of supersaturations (e.g., Fig. 3) to determine E, C, and s^* for each particle size during a supersaturation cycle. Resulting fits were then filtered to assure reasonable fit values with the criteria that $0.2 < E < 1.2$ and $-15 < C < -2$; values of $C > -2$ no longer provide a physically realistic sigmoid (Appendix A) and values of $C < -15$ are limited by instrument resolution (Lance, 2007; Appendix A). χ^2 values, a measure of the goodness of the fit, are obtained, and the highest 5 % are filtered to remove the outliers. Using these filter criteria, the percentage of discarded fits for 40, 60, and 80 nm data are ∼14 %, 10 %, and 16 %, respectively.

$R_a(s)$ represents a cumulative distribution of critical supersaturation for particles with dry diameter d_p. Assuming that this variability is driven solely by variance in chemical composition, we can transform $R_a(s)$ into a cumulative distribution of hygroscopicity, $R_a(\kappa)$, using the definition of κ (if $\kappa >\sim 0.1$),

$$\kappa = \frac{4A^3}{27 d_p^3 s^{-2}} \tag{3}$$

where d_p is the dry diameter of the particle (Petters and Kreidenweis, 2007).

For every s^* there is a corresponding characteristic hygroscopicity parameter, κ^*, so that (s/s^*) can be expressed as $(\kappa/\kappa^*)^{-1/2}$. From this and Eq. (2), the complement of $R_a(s)$ can be written as

$$R_a(\kappa) = E - \frac{E}{1+\left(\frac{\kappa}{\kappa^*}\right)^{-\frac{C}{2}}} = \frac{E}{1+\left(\frac{\kappa}{\kappa^*}\right)^{\frac{C}{2}}} \tag{4}$$

The probability distribution function (PDF) for κ, $p^s(\kappa)$ can be found by differentiating Eq. (4) with respect to κ and normalizing over the integral of possible κ values.

$$p^s(\kappa) = \frac{1}{E}\frac{dR_a(\kappa)}{d\kappa} = -\frac{\frac{C}{\kappa^{*2}}\left(\frac{\kappa}{\kappa^*}\right)^{\frac{C}{2}-1}}{\left(1+\left(\frac{\kappa}{\kappa^*}\right)^{\frac{C}{2}}\right)^2} \tag{5}$$

Analysis of $p^s(\kappa)$ can provide the chemical dispersion, which describes the degree of chemical heterogeneity of the CCN population. As described in Lance (2007), the chemical dispersion, $\sigma(\kappa)$, of particles of size d_p can be found by computing the square root of variance about κ^* (assuming a Gaussian distribution where the average κ is equal to κ^*)

$$\sigma^2(\kappa) = \frac{\int_0^\infty (\kappa-\kappa^*)^2 p^s(\kappa) d\kappa}{\int_0^\infty p^s(\kappa) d\kappa} \tag{6}$$

so that the chemical heterogeneity of the CCN population can be approximated by $\kappa^* \pm \sigma\ (\kappa)$. Thus, the chemical dispersion is described by the spread in the distribution of measured κ values, illustrating the degree of heterogeneity in particle chemistry. Further explanation of this method, including a discussion on the chosen integration limits of 0 to 1 used in Eq. (6) and the contribution of instrument operation on $\sigma(\kappa)$ are discussed in Appendix A.

4 Results

Temporal variation of HTDMA-derived and CFSTGC-derived κ values, total particle concentration, and AMS mass concentrations throughout the campaign are shown in Fig. 4. Error bars (see Appendix A) are not shown, because these are usually small and difficult to discern in the figure. Average uncertainties for κ values are 0.009, 0.012, and 0.021 for 40, 60, and 80 nm particles, respectively. CN concentrations are typically below 200 particles cm^{-3} for 40, 60, and 80 nm particles, and AMS total mass ranges from 0 to 10 $\mu g\, m^{-3}$. While during some periods these quantities show similar trends (e.g., 4/9/2007 to 4/11/2207 and 5/1/2007 to 5/11/2007), correlation of these parameters with κ variability is weak. The trend in κ values derived from HTDMA and CFSTGC measurements correlate well (as discussed in the following). General trends of κ values for different size particles are very similar, although specific differences between sizes will be presented in the following analysis. Average CFSTGC-derived κ values for 40, 60, and 80 nm particles are 0.20 ± 0.06, 0.19 ± 0.06, and 0.22 ± 0.06, respectively, while average HTDMA-derived κ values for 30 and 50 nm particles are 0.15 ± 0.06 and 0.14 ± 0.05, respectively. As aerosol aqueous-phase solutions in the HTDMA are more concentrated than those in the CFSTGC and calculations of κ may be more greatly impacted by solution non-ideality, phase separation, and partial solubility of constituents, it is not surprising that HTDMA-derived κ averages are generally lower. Also, the CCN counter detects only those particles that are activated (as indicated by the E parameter) which means that non-hygroscopic particles do not impact the slope of the sigmoid used to calculate s^*. When the HTDMA detects non-hygroscopic particles, it results in a GF = 1 which invariably decreases the inferred value of κ. However, as E is almost always >0.9, the contribution of non-hygroscopic particles to the HTDMA-derived κ is small. A likely reason for the differences seen is that a larger fraction of the commonly less soluble organic material is dissolved in the dilute droplets present in the CFSTGC. HTDMA-derived κ values from this study are in agreement with the HTDMA-derived average $\kappa = 0.18$ for 35, 50, 75, and 110 nm particles reported for this region by Sihto et al. (2010) for July 2008 to June 2009. The slight discrepancy between our results and those reported by Sihto et al. (2010) may result from the fact that particle hygroscopicity in this region is dependent on particle size (e.g., Birmili et al., 2009) and larger particles typically show increased hygroscopicity (also shown by the higher average CFSTGC-derived κ for 80 nm particles compared to that of 60 and 40 nm particles discussed in Sect. 4.2).

Comparison of κ values from 60 nm CCN data against 50 nm HTDMA data for the entire campaign is presented in Fig. 5. The higher magnitude of CFSTGC-derived over HTDMA-derived κ values is again seen in this comparison with most of the values consistent within ±30 %. As discussed above, these differences are well within the range

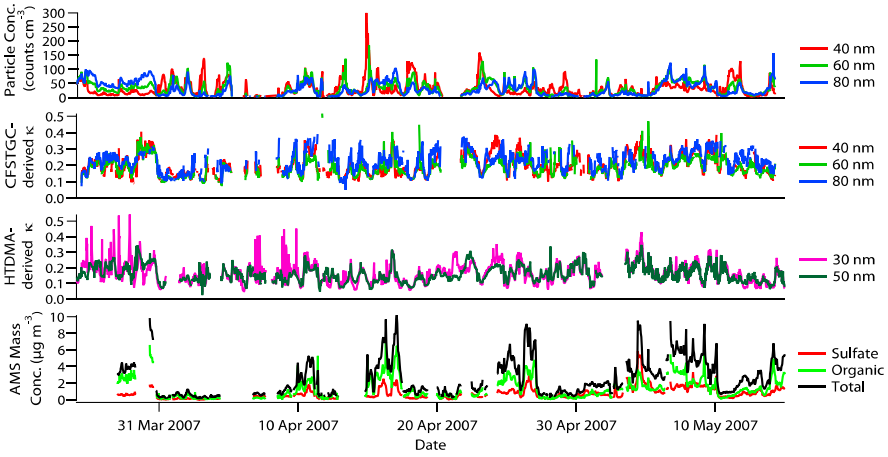

Fig. 4. Temporal variation of HTDMA-derived and CCN-derived κ values, total particle concentration, and AMS mass concentration throughout the campaign.

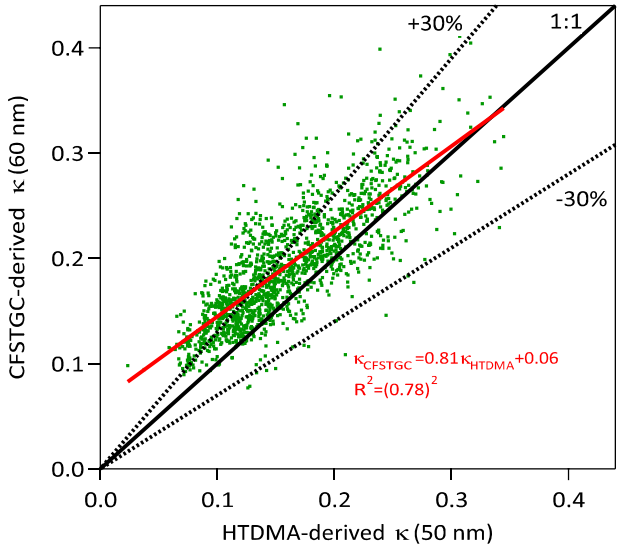

Fig. 5. CFSTGC-derived κ values for 60 nm diameter particles against HTDMA-derived κ values for 50 nm diameter particles. Shown is a best fit line (red), 1:1 line (black, solid), and lines of $\pm$30 % deviation (black, dotted).

of possible uncertainties often seen between HTDMA and CFSTGC-derived κ values (e.g., Petters and Kreidenweis, 2007; Prenni et al., 2007, 2009; Massoli et al., 2010).

4.1 Diurnal variability of CCN properties

Diurnal variation in CCN maximum activated fraction (E) and characteristic critical supersaturation (s^*) are shown for 40, 60, and 80 nm particles (Fig. 6a and b). The error bars represent day-to-day variations, which are greater than the average fitting uncertainties (see Appendix A). For example, the average fitting uncertainties for the maximum activated fraction are 0.04, 0.02, and 0.02 for 40, 60, and 80 nm particles, respectively, and those for the characteristic critical supersaturation are all 0.02 %. While the 60 and 80 nm particles show rather constant values of E, 40 nm data seem to display a decrease in E the from late morning through evening (Fig. 6a). This daytime decrease in maximum activated fraction, however, is the result of not reaching the asymptote for 40 nm spectra at the highest supersaturation measured ($s_{\max}$). If calculations are repeated using $R_a(s_{\max})$ instead of the asymptote $E = R_a(\infty)$, this diurnal cycle is no longer apparent. Thus, it is expected that the true diurnal variation of E for 40 nm particles is analogous to that of the 60 and 80 nm particles. Not reaching the asymptote, however, has negligible effects, if any, on the C and s^* fit parameters. As expected, 40 nm particles have the highest characteristic critical supersaturations of the particle sizes sampled in this study and reach their critical supersaturation well below the highest instrument supersaturation ($\sim$1.8 %) (Fig. 6b). Diurnal trends in total particle concentration, corrected to account for dilution air added to the sample flow, are similar for all measured sizes (Fig. 6c).

4.2 Diurnal variability of κ

Diurnal trends in CFSTGC-derived and HTDMA-derived κ values are seen for all particle sizes sampled with minimum κ values occurring in the early morning (near sunrise) and maximum κ values occurring in the afternoon (Fig. 7a and c). This diurnal trend corresponds well with those found by previous studies at the Hyytiälä site (e.g., Hämeri et al., 2001; Väkevä et al., 2002; Boy et al., 2004; Ehn et al., 2007). CFSTGC-derived κ values covary with AMS-derived inorganic volume fraction, daily temperature trends, and AMS f_{44} data. As f_{44} increases linearly with O/C ratio (Aiken et

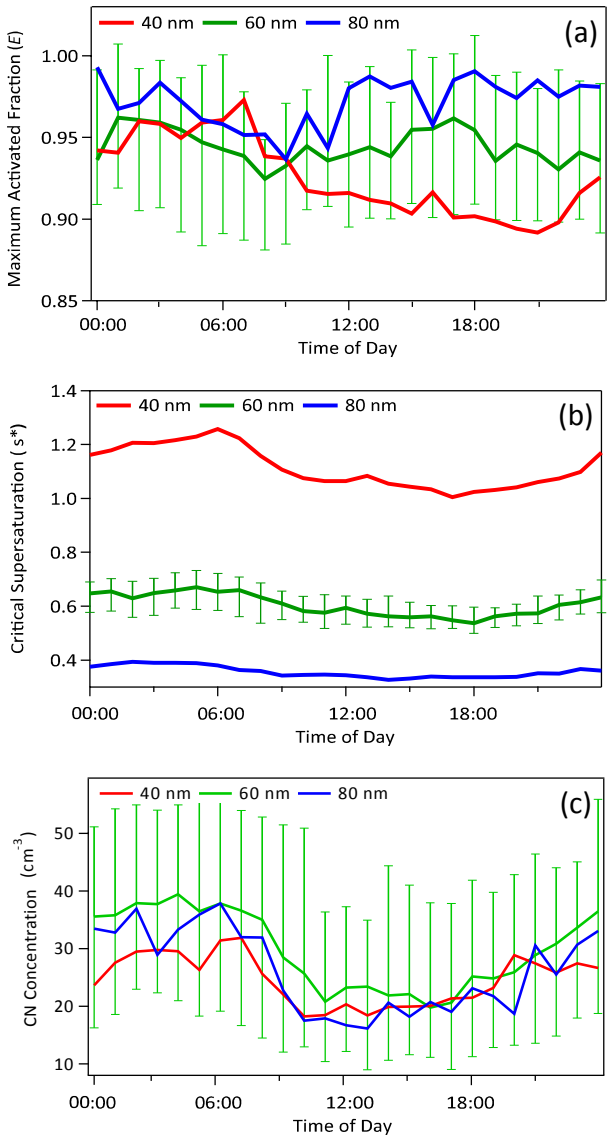

Fig. 6. Diurnal variation of the **(a)** CCN maximum activated fraction, **(b)** critical supersaturation, and **(c)** CN concentration for 40, 60, and 80 nm particles. Solid lines represent median values. Bars representing the 25th and 75th percentile values are shown for 60 nm data.

al., 2008) and organics in the atmosphere typically become more oxidized as they age; this suggests that aerosol hygroscopicity is also determined by the aging of those organics. This is consistent with the view of oxidation state correlating with hygroscopicity presented by Jimenez et al. (2009) and Massoli et al. (2010).

As reported by Boy et al. (2004), GF (related to κ by Eq. 1) is more variable during the daytime than the early morning period. This is also observed in our study as there is typically a clear peak in normalized κ frequency in the early morning while there is a wide spread of κ values with no clear peak in the afternoon (Fig. 7b). The clear size-dependence shown by Boy et al. (2004) is also seen in our diurnal κ trend, as larger particles display larger κ values than the smaller particles (Fig. 7c). Our observations confirm the different hygroscopic modes reported by Hämeri et al. (2001) where Aitken mode particles (35, 50, and 73 nm) show distinctly different hygroscopic behavior than the larger accumulation mode particles (about 80 nm or larger).

The chemical dispersion, $\sigma(\kappa)$, describing the degree of heterogeneity in particle chemistry, for 40, 60, and 80 nm particles is shown in Fig. 8. 60 and 80 nm particles show a potential diurnal trend in chemical dispersion, similar to that of diurnal κ. Chemical dispersion of 40 nm particles, however, remains rather steady and does not show the same increase just before noon as observed for the other sizes. The composition of nucleation and Aitken mode particles are influenced by nucleation events (Hämeri et al., 2001); it is therefore possible that 40 nm particles do not experience the afternoon increased chemical dispersion since new particle formation events often occur around noon (Nieminen et al., 2009). This means that while the chemical dispersion of larger particles changes, these 40 nm particles still reflect the composition of newly formed particles originating in the boreal forest. As 60 nm particles exhibit a similar diurnal κ trend (Fig. 7c), one might initially expect similar chemical dispersion. However, 60 nm particles (and larger) would have had more time to be affected by SOA condensation, coagulation, and long range transport; thus, they may exhibit a larger degree of chemical heterogeneity than 40 nm particles. This is in agreement with Petäjä et al. (2005) who showed remarkable variability in the Aitken mode hygroscopicity which was linked to air mass transport and indirectly possibly to aging while, on the other hand, showed that the nucleation mode hygroscopicity was quite constant due to relatively homogeneous surroundings. This is also consistent with Hämeri et al. (2001) whom also saw that external mixing increases with increasing particle size in Hyytiälä.

Current values of relative chemical dispersion are similar to those from a megacity environment (Su et al., 2011). The magnitude of chemical dispersion depends somewhat on hygroscopicity, so relative values, $\sigma(\kappa)/\kappa$, are used for comparison. Further details regarding the comparison are given in Appendix A, and the chemical dispersion values are given in Table A2. Based on the average $\sigma(\kappa)$ and κ, current relative chemical dispersion values for the 40, 60, and 80 nm dry size are 0.55, 0.63, and 0.77, respectively, and those from Su et al. (2011) for 39, 55, and 75 nm dry size are 0.60, 0.50, and 0.54, respectively. Deviations are seen at larger particle sizes, but considering the uncertainties related to the interpretation of chemical variability (e.g., DMA transfer function effects, etc. as described in Appendix A and Lance et al., 2007) firm conclusions cannot be made.

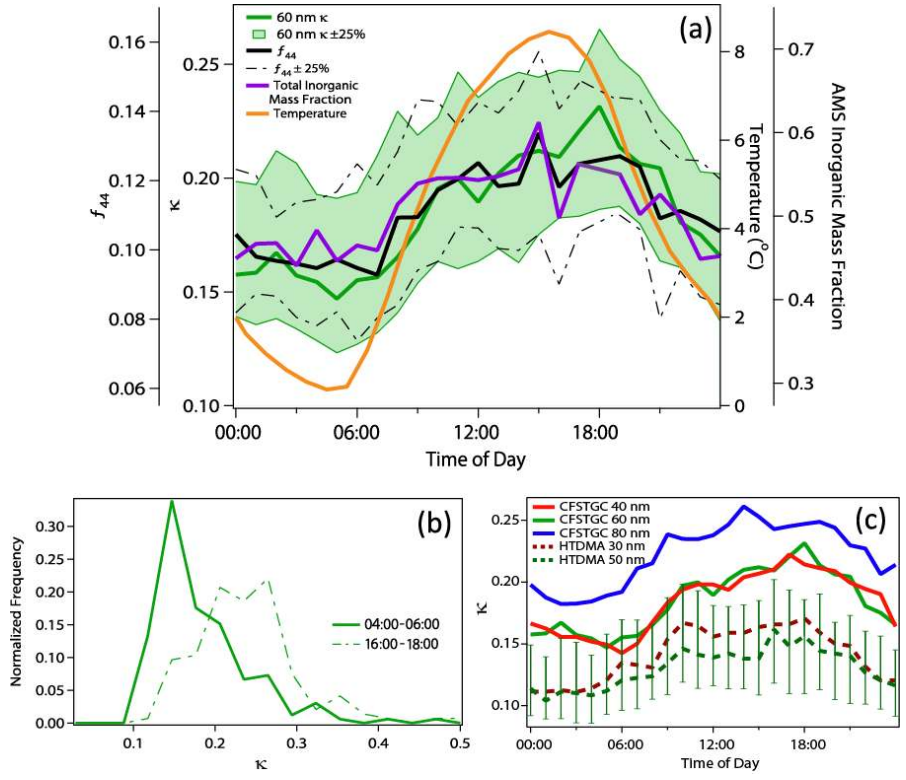

Fig. 7. **(a)** Diurnal trend of 60 nm CFSTGC-derived median κ (green line) with 25th and 75th percentiles shaded in green. Also shown are average temperature (orange line), median f_{44}, given by AMS (black line) with 25th and 75th percentiles shown by dotted black lines, and median inorganic mass fraction (purple line). **(b)** Frequency distributions of 60 nm CFSTGC-derived κ values for times of minimum (solid line) and maximum (dotted line) κ values. **(c)** Diurnal CFSTGC-derived κ distributions for 40, 60, and 80 nm particles and HTDMA-derived distributions for 30 and 50 nm particles. Bars representing the 25th and 75th percentile values are shown for 60 nm and 50 nm data.

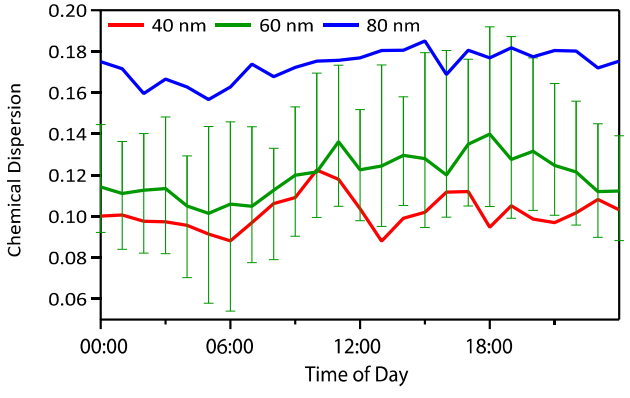

Fig. 8. Diurnal variation of $\sigma(\kappa)$ for 40, 60, and 80 nm particles.

4.3 On κ closure with AMS data

κ, which represents the overall aerosol hygroscopicity, is the sum of contributions from each aerosol constituent

$$\kappa = \sum\nolimits_j \kappa_j \varepsilon_j \tag{7}$$

where ε_j and κ_j are the volume fraction and hygroscopicity parameter, respectively, of aerosol component j (Petters and Kreidenweis, 2007). Based on AMS data, the components can include organic and inorganic salts calculated from the measured ion concentrations (e.g., Raatikainen et al., 2010). When there are no significant variations in the composition of the organic and inorganic fractions (as seems to be the case in this data set) only the inorganic and organic fraction are needed for a reasonably good prediction

$$\kappa = \varepsilon_i \kappa_i + \varepsilon_0 \kappa_0 \tag{8}$$

where ε_i and ε_0, and κ_i and κ_0, are the volume fraction and hygroscopicity parameters of inorganics and organics, respectively. Fits were also tested for a three component model that includes inorganic ions as one group as well as the more and less oxidized organic groups. This model was shown to be superior during a previous campaign in 2005 (Raatikainen et al., 2010), but in the current campaign the average organic mass fractions are lower and there are much less variations in organic oxidation state. As a result, predictions for the three component approach provided similar results to the two component model, which will be used in

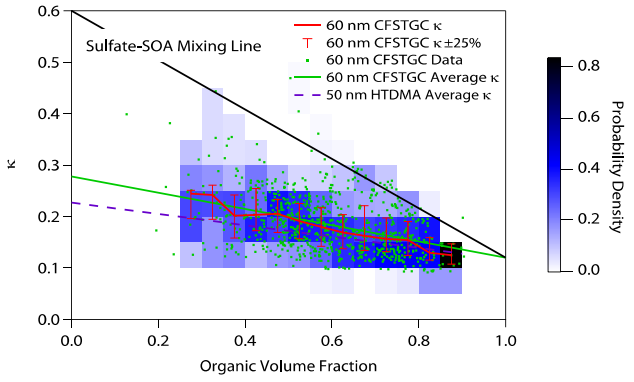

Fig. 9. 60 nm CFSTGC-derived κ median values (red line) with bars showing 25th and 75th percentiles. Actual 60 nm CFSTGC-derived κ values shown by green circles. Probability density for 60 nm data is indicated by the blue shading. The black dashed line indicates the sulfate-SOA mixing line. The solid green line shows the average value of 60 nm CFSTGC-derived κ as predicted by AMS closure while the dashed purple line shows the 50 nm HTDMA-derived κ as predicted by AMS closure.

Table 1. κ_o and κ_i values for 40, 60, and 80 nm particles.

Particle Size (nm)	κ_o	κ_i
40	0.12	0.30
60	0.12	0.30
80	0.14	0.35

this study. The relevant inorganic ions detected by the AMS include ammonium, nitrate, and sulfate. In order to find volume fraction, their mass concentrations were combined and, as ammonium sulfate dominated the inorganic mass, the density of ammonium sulfate, 1.77 g cm^{-3}, was assumed (Lance et al., 2009). Organic volume was calculated using a density of 1.4 g cm^{-3} and measured mass concentrations (Lance et al., 2009). 60 nm CFSTGC-derived κ values and a linear fit based on the 50 nm HTDMA-derived κ values as a function of AMS measured organic volume fraction are shown in Fig. 9. Typical expected κ values for a pure inorganic compound (i.e., ammonium sulfate) as well as pure SOA are shown by the sulfate-SOA mixing line.

Fitted κ_i and κ_o for 40, 60, and 80 nm particles are shown in Table 1. The higher magnitude of both of these values for 80 nm data is expected as the general magnitude of hygroscopicity is greater for this size than for 40 and 60 nm particles (Fig. 7c). Still, while these values correspond well with the κ_o value of 0.1 used in Sihto et al. (2010) and proposed by Gunthe et al. (2009), κ_i values are too low for typical inorganic compounds as the hygroscopicity of ammonium sulfate is ~0.6 (Petters and Kreidenweis, 2007). Bulk mass concentrations measured by the AMS during the campaign were dominated by particles with volume diameter typically ranging from about 300–400 nm (mean volume diameter ~380 nm), much greater than those sampled by the CFSTGC. Since large particles have been shown to differ in hygroscopicity and chemical dispersion from smaller particles and the organic mass fraction in Aitken particles has been shown to be significantly higher than in larger particles (Allan et al., 2006), bulk composition measurements (in this case from AMS) may overestimate the inorganic mass fraction used to describe the 40, 60, and 80 nm particles in this study. These results illustrate that bulk composition measurements should be used with caution as they may sometimes be inadequate when applied to the study of particles of CCN-relevant sizes.

4.4 CCN activation kinetics

The droplet diameter of a given particle exposed to a constant supersaturation in the CFSTGC is described by (Lance et al., 2006; Lathem and Nenes, 2011),

$$D_p^2 = D_0^{*2} + 2G \int_{t_{act}}^{t_{out}} s dt \quad (9)$$

where D_p is the droplet diameter exiting the CFSTGC, D_0^* is the diameter of the CCN when exposed to its critical supersaturation, s_c, t_{act} is the time (after entrance in the growth chamber) when the supersaturation in the instrument becomes equal to s_c, and, t_{out} is the time when droplets exit the growth column. G is a coefficient that encompasses mass and heat transfer properties of the particle (Roberts and Nenes, 2005; Lance et al., 2006). From Eq. (9), D_p tends to increase with increasing s. This is shown by the range of 80 nm particle D_p throughout the study in Fig. 10a, where D_p is color-coded by instrument s. The second term in Eq. (9) dominates over the first term for particles of low s_c, so that the droplet size at the exit of the instrument is insensitive to its s_c. This effect is shown in Fig. 10b for all size-selected particle sizes, each with a respective s^*, where D_p become increasing similar at the highest s values. This also means that droplet size distributions narrow at increasing supersaturation (as illustrated by the vertical error bars in Fig. 10b and the narrowed droplet size distribution at high s values in Fig. 10b). However, the asymptotic size reached by the particles at high s (Fig. 10b) is a result of the compensating effects between a higher s and a larger entry length required for its development (i.e., t_{act} approaches t_{out} as instrument s increases; Lance et al., 2006).

Threshold Droplet Growth Analysis (TDGA) is a method used to investigate shifts in droplet growth kinetics for ambient (Bougiatioti et al, 2009, 2011; Lance et al., 2009; Padró et al., 2010) and laboratory (Engelhart et al., 2008; Asa-Awuku et al., 2009, 2010, 2011) aerosol. The average droplet diameter of particles exiting the CFSTGC is measured and compared to droplet size from calibration aerosol (typically ammonium sulfate or sodium chloride) with s_c equal to the

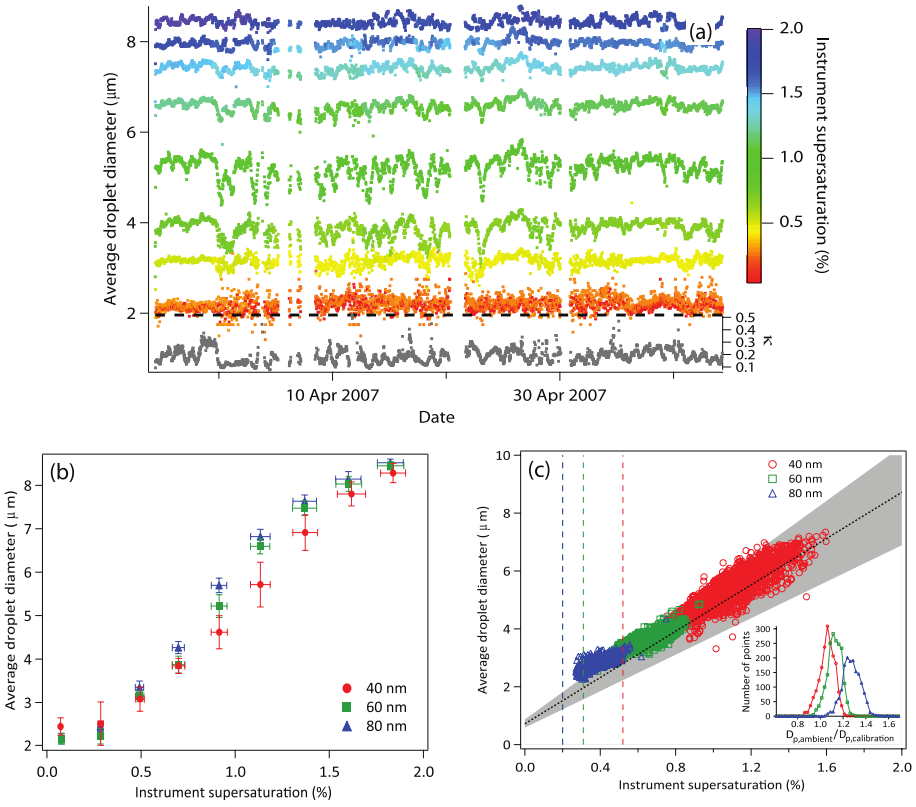

Fig. 10. **(a)** Temporal variation of droplet size for ambient 80 nm particles color-coded by instrument supersaturation. κ values are shown in grey (right-hand scale). **(b)** Average droplet diameters for 40 (red circles), 60 (green squares), and 80 nm (blue triangles). Vertical and horizontal error bars represent the standard deviation of measured droplet sizes and supersaturation, respectively. **(c)** Activated droplet sizes for 40 (red circles), 60 (green squares), and 80 nm (blue triangles) ambient particles measured at supersaturations closest to the critical supersaturation of ammonium sulfate particles of the same respective size. The calibration curve is shown by a black dotted line while the grey area indicates the sizing uncertainty for the ammonium sulfate particles. Critical supersaturations for 40, 60, and 80 nm ammonium sulfate particles are given by red, green, and blue dashed lines, respectively. Inset are histograms for each size particle indicating the occurrence of ratios of ambient wet droplet size to calibration wet droplet size.

instrument supersaturation. Calibration aerosol represents an upper limit of rapid activation kinetics, as the material is deliquesced before it activates and the water vapor uptake coefficient is large. Therefore, if ambient aerosol experience rapid activation kinetics, the droplet sizes of ambient and calibration particles should be similar. Provisions should be taken to avoid high CCN concentrations in the instrument that would deplete s and affect D_p, with implications on droplet size (Lathem and Nenes, 2011).

The calibration of the CFSTGC in this study was carried out with SMCA (Moore et al., 2010). In addition to a highly accurate calibration curve, the method also provides D_p for a wide range of particle sizes and s^*. Figure 10c shows D_p for 40, 60, and 80 nm particles at $s = s^*$ and lines based on average D_p of calibration aerosol. As the instrument did not sample particles directly at their s^* but rather for set steps on instrument supersaturation, the two supersaturation values and wet diameters closest to s^* were used in interpolating the droplet diameter at s^*. Average droplet sizes from ambient aerosol grow to sizes comparable to calibration aerosol. This means that the organics present at Hyytiälä are not associated (on average) with retarded activation kinetics. A small fraction (<10 % of the total CCN) did exhibit significantly smaller droplet sizes than the calibration aerosol.

5 Conclusions

The size-resolved hygroscopicity and activation kinetics were investigated for particles sampled at the SMEAR II boreal forest station in Hyytiälä, Finland, from March to May 2007. CCN maximum activated fraction show similar values for 60 and 80 nm aerosol and remain close to unity. Although results of maximum activated fraction of 40 nm particles were impacted by the range of supersaturations measured in this study, these particles are expected to show variation similar to that of 60 and 80 nm particles.

Overall, κ values are mainly found between 0.10 and 0.40 for all sizes with an average of 0.20 ± 0.06, 0.19 ± 0.06,

and 0.22 ± 0.06 for 40, 60, and 80 nm particles, respectively. These low values reflect the dominant role of organics on CCN activity. The diurnal trend of κ with inorganic volume fraction and f_{44} suggests that κ variability may be partly explained by the diurnal variability of organics in the atmosphere and particle aging. This suggests that the trend in organic composition and oxidation state of both small CCN-relevant size particles and larger particles sampled in bulk measurements is the same and also that more aged (oxidized) particles have higher hygroscopicities than less oxidized organics.

The diurnal trend in κ displays maximum values in the afternoon and minimum values in the early morning as has been seen in previous studies by Hämeri et al. (2001), Väkevä et al. (2002), Boy et al. (2004), and Ehn et al. (2007). The high variability of afternoon κ values and the general increase in κ observed for larger particles confirm the results of these earlier studies. 60 and 80 nm particles show a slight diurnal trend in chemical dispersion while 40 nm dispersion remains rather stable. This could be representative of the effect of new particle formation on the chemical composition of 40 nm particles and also the effect of increased external mixing with size.

Hygroscopicity of the aerosol organic and inorganic fractions were predicted from bulk composition (using an AMS) and CCN-derived aerosol hygroscopicity. Hygroscopicity of the inorganic fraction was considerably lower than expected, which indicates that bulk measurements should be used with caution for representing characteristics of small mode particles. Due to the high number of nucleation events at the SMEAR II station, the composition of small particles (which contribute significantly to CCN concentrations) differs from that of large particles (which are more closely represented by measurements of bulk composition).

Analysis of droplet growth kinetics shows that ambient particles activate and grow as rapidly as calibration aerosol, adding to an emerging body of evidence that highly oxidized organics (even if they constitute the majority of the aerosol volume) do not inhibit the rate of water uptake. If this is representative of other locations and seasons, it will substantially simplify the description of CCN activation kinetics in atmospheric models of aerosol-cloud-climate interactions.

Appendix A

Analysis of hygroscopicity distributions

There are several assumptions made in using and analyzing results from the PDF in Eq. (5) in order to arrive at appropriate, meaningful results for $\sigma(\kappa)$. An important issue regards the sigmoidal fit function, as it can yield non-negligible probability for atmospherically irrelevant κ (Fig. A1). For example, in Eq. (4), when κ is ten times greater than κ^* and $C = -2$, then $R_a(\kappa) = 0.9E$, which means that there is a

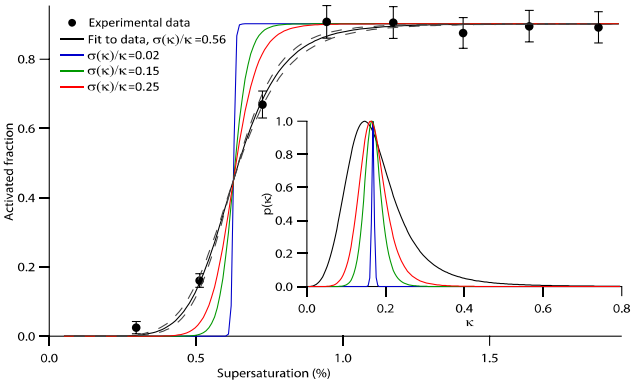

Fig. A1. An example of measured and fitted activation spectrum (60 nm dry size, 4/14/2007, 18:55:00) and three examples of activation spectra with different $\sigma(\kappa)$ values. Corresponding κ distributions are shown in the inset. Error bars represent Poisson counting uncertainties.

Table A1. Average uncertainty values for fitted (s^*, E, and C) and derived (κ, $\sigma(\kappa)$ and $\sigma\ (\kappa)/\kappa$) parameters.

Particle Size (nm)	s^*	E	C	κ	$\sigma(\kappa)$	$\sigma(\kappa)/\kappa$
40	0.023	0.036	0.98	0.009	0.013	0.074
60	0.018	0.024	1.26	0.012	0.019	0.115
80	0.017	0.023	1.72	0.021	0.026	0.151

10 % probability that $\kappa > 10\kappa^*$. This is unrealistic for ambient data collected during the campaign. We have filtered the data to exclude distributions for which $C > -2$ as this kind of flat activation curve is often strongly influenced by multiply charged particles. On the other hand, values of $C < -15$ were filtered, because any values lower than -15 means that activation cannot be resolved with a supersaturation step size of 0.2 %. This also happens to be the practical limit for the lowest observed C from instrument calibration experiments where higher resolution can be used. A small fraction of the data is subject to these issues and has a minimal impact on the results. We have also chosen to implement a constant upper limit for integration of 1 as this is the upper limit of atmospherically-relevant κ values (except for sea salt, whose $\kappa \approx 1.2$ (Petters and Kreidenweis, 2007)) and well above those seen in Hyytiälä during this campaign.

Instrument operation also induces some broadening of $R_a(s)$ and $R_a(\kappa)$ and contributes to $\sigma(\kappa)$. An ideal instrument sampling a chemically homogenous mixture of monodisperse particles would result in $R_a(\kappa)$ being a step function with $\sigma(\kappa) = 0$ and $C = -\infty$. In reality, the finite width of the DMA transfer function (Wang and Flagan, 1990) and a corresponding transfer function in the CFSTGC from exposure to a finite range of supersaturations, the assumption of particle sphericity, and fluctuations in instrument operation

Table A2. Comparison of data with Su et al. (2011).

Cerully et al. (2011)				Su et al. (2010)					
Size (nm)	κ	$\sigma(\kappa)$	$\frac{\sigma(\kappa)}{\kappa}$	Size (nm)	κ_g	κ	$\sigma_g(\kappa)$	$\sigma(\kappa)$	$\frac{\sigma(\kappa)}{\kappa}$
40	0.20 ± 0.06	0.11 ± 0.04	0.55	39	0.30	0.35	1.74	0.21	0.60
60	0.19 ± 0.06	0.12 ± 0.05	0.63	55	0.38	0.42	1.60	0.21	0.50
80	0.22 ± 0.06	0.17 ± 0.04	0.77	75	0.47	0.54	1.67	0.29	0.54

(i.e., flow rate and temperature) all induce a broadening of the response to give a finite, but still steep slope for $R_a(s)$.

In practice, the inferred $\sigma(\kappa)$ contains a fairly constant instrument offset and a strongly time-dependent component that represents the actual chemical variability. In terms of $\sigma(\kappa)/\kappa$, most of the observed values in Hyytiälä are between 0.25 and 1.3, so the instrument offset ($\sim$0.25) is rather small compared to the effect of chemical variability. As the first step to explain the instrument offset for $\sigma(\kappa)/\kappa$ ($\sim$0.25) we have estimated the magnitude of instrument supersaturation fluctuations. For example, the upper limit for instrument supersaturation fluctuations due to variations in CFSTGC temperatures was found to be $\sigma(s)/s = 0.01$. Based on Eq. (3), $\sigma(\kappa) = (\mathrm{d}\kappa/\mathrm{d}s)\sigma(s) = 2\kappa/s\sigma(s)$, which means that $\sigma(\kappa)/\kappa = 0.02$. This is a small value compared with the lowest observed value of 0.25, and under normal operation supersaturation fluctuations can be considered as a second order effect. Several other possibilities such as fluctuations in pressure and inlet RH were also considered, but these are found to have even smaller contribution to the instrument $\sigma(\kappa)$.

As shown by Lance (2007), the DMA transfer function results in significant spread to the activation spectrum. For example, the relative width of the DMA transfer function (Wang and Flagan, 1990) for a 4.5:1 sheath-to-aerosol flow ratio is roughly $\sigma(D_p)/D_p = 0.053$. Again, an order of magnitude approximation based on Eq. (3) shows that $\sigma(\kappa)/\kappa = 3 \times 0.053 = 0.16$. Another important contribution to the spread in the activation spectrum comes from multiply charged particles as these larger particles activate at lower supersaturations. There are no simple ways to estimate this effect, because the fraction of multiply charged particles depends on charging probability and size distribution at the charger, which is not always known and hardly ever constant. When expecting uniform particle distribution at the charger, accounting for multiply charged particles (Gunn, 1956; Wiedensohler and Fissan, 1988) and DMA transfer function effects (Wang and Flagan, 1990) increases $\sigma(\kappa)/\kappa$ for 80 nm particles to about 0.2, but the effect is negligible for 40 nm particles. As a result, the DMA transfer function explains 64–80 % of the observed $\sigma(\kappa)$ offset. The unexplainable fraction of the $\sigma(\kappa)$ offset is caused by a combination of several second order effects such as CFSTGC transfer function, diffusion widening of the size distributions, and using the simplified hygroscopicity approach (Eq. 3).

Figure A1 shows an example of a typical fitted activation curve based on ambient observations and calculated activation curves for different $\sigma(\kappa)/\kappa$ values mentioned above. It can be seen that the steepest detected distributions ($\sigma(\kappa)/\kappa$=0.25) are similar to the distribution based only on the DMA transfer function ($\sigma(\kappa)/\kappa$=0.16). In addition, ambient distributions can usually be clearly distinguished from the instrument limit ($\sigma(\kappa)/\kappa = 0.25$).

To conclude, the $\sigma(\kappa)$ values include various effects of normal operation uncertainties, dominated by the DMA transfer function. With the exception of the multiply charged particles, these effects are practically time and size invariant. This means that calculated $\sigma(\kappa)$ values contain a fairly constant instrument offset (roughly 0.25 in the current data), but the remaining, much larger variations (from 0.25 to well above 1) can be related to chemical variability. More comprehensive methods exist for separating variability in particle size and composition (e.g., Lance, 2007; Su et al., 2010), but the current method is a very good approximation and very simple to implement.

The error bars in activation ratios (Fig. A1) represent Poisson counting uncertainties, which are equal to the square root of the number of observed counts. It would be possible to use these uncertainties as weights when fitting the sigmoid and in the error analysis after the fitting, but here we have used the more "traditional" approach of assuming equal weights and computing parameter uncertainties from the residual. For most activation curves, both fitting methods give similar predictions; in the example of Fig. A1, $E = 0.902 \pm 0.013$, $C = -7.78 \pm 0.73$, and $s^* = 0.628 \pm 0.011$ assuming equal weights, while $E = 0.903 \pm 0.022$, $C = -7.52 \pm 0.81$, and $s^* = 0.627 \pm 0.014$ for the weighted fit. Significant differences in the fitted parameters are seen only when the fits are poorly constrained by the data.

Error analysis can be used to estimate the net effect of uncertainties. Chemical variability, $\sigma(\kappa)$, is calculated from Eq. (6), and it depends on characteristic hygroscopicity (κ^* or just κ from now on) and C. When dry particle diameter and temperature uncertainties are assumed negligible, κ uncertainty depends only on that of critical

supersaturation (Δs):

$$\Delta(\kappa) = \left| \frac{\partial \kappa}{\partial s} \Delta(s) \right| = 2\frac{\kappa}{s}\Delta(s) \quad \text{(A1)}$$

Chemical variability is an integral function, so closed form expression cannot be derived for the uncertainty. Uncertainties of C and κ must be propagated using numerically calculated gradients.

$$\Delta(\sigma(\kappa)) = \sqrt{\left(\frac{\partial \sigma(\kappa)}{\partial C}\Delta(C)\right)^2 + \left(\frac{\partial \sigma(\kappa)}{\partial \kappa}\Delta(\kappa)\right)^2} \quad \text{(A2)}$$

For the relative chemical variability, $\sigma(\kappa)/\kappa$, the uncertainty in κ must also be accounted for.

$$\Delta(\sigma(\kappa)/\kappa) = \sqrt{\left(\frac{1}{\kappa}\Delta(\sigma(\kappa))\right)^2 + \left(\frac{\sigma(\kappa)}{\kappa^2}\Delta(\kappa)\right)^2} \quad \text{(A3)}$$

Average uncertainties are shown in Table A1. Uncertainties of s, E and C are based on fitting while those of the derived quantities (κ, $\sigma(\kappa)$ and $\sigma(\kappa)/\kappa$) are calculated using Eqs. (A1) through (A3).

Few data are available for comparison of $\sigma(\kappa)/\kappa$ values; uncertainty between instrument offsets and the effect of ambient size distributions may induce additional uncertainty on the inferred chemical variability. However, Su et al. (2011) found quite similar values for a megacity environment, indicating that variability between instruments are not dominating. The same study obtained log-normal hygroscopicity distribution parameters for several constant instrument supersaturations (see Table 1 in Su et al., 2011). Arithmetic distribution parameters were calculated from the log-normal parameters and the activation dry particle sizes were calculated from the mean hygroscopicity parameter and supersaturation (solved from Eq. 3) values. The results for the three closest dry particle sizes are shown in Table A2. While our values indicate increasing $\sigma(\kappa)/\kappa$ as a function of dry particle size, there is a weaker opposite trend in the Su et al. (2011) data. Clear deviations are seen at the larger particle sizes, which possibly reflect true compositional variability between megacity and boreal forest environments.

Acknowledgements. We acknowledge Jack Lin and Pulin Patel for assistance in some intermediate data processing as well as all those involved in the EUCAARI campaign and SMEAR II site. Support for this research was provided by NSF CAREER and NCAR-ASP grants as well as the Finnish Cultural Foundation. Additionally, the financial support by the Academy of Finland Centre of Excellence program (project no 1118615), EU project FP7-ATMNUCLE project No. 227463 (ERC Advanced Grant), and EU-project EUCAARI (European Integrated project on Aerosol Cloud Climate and Air Quality interactions, project no 036833-2) is gratefully acknowledged. T. Petäjä acknowledges funding from the Nessling Foundation (2010143) and Academy of Finland (139656).

Edited by: K. Carslaw

References

Aalto, P. and Kulmala, M.: Using a cloud condensation nuclei counter to study CCN properties and concentrations, Boreal Env. Res., 5, 349–359, 2000.

Aiken, A. C., DeCarlo, P. F., Kroll, J. H., Worsnop, D. R., Huffman, J. A., Docherty, K., Ulbrich, I. M., Mohr, C., Kimmel, J. R., Sueper, D., Zhang, Q., Sun, Y., Trimborn, A., Northway, M., Ziemann, P. J., Canagaratna, M. R., Onasch, T. B., Alfarra, R., Prevot, A. S. H., Dommen, J., Duplissy, J., Metzger, A., Baltensperger, U., and Jimenez, J. L.: *O/C* and *OM/OC* ratios of primary, secondary, and ambient organic aerosols with high-resolution time-of-flight aerosol mass spectrometry, Environ. Sci. Technol., 42, 4478–4485, 2008.

Alfarra, M. R., Coe, H., Allan, J. D., Bower, K. N., Boudries, H., Canagaratna, M. R., Jimenez, J. L., Jayne, J. T., Garforth, A. A., Li, S.-M., and Worsnop, D. R.: Characterization of urban and rural organic particulate in the Lower Fraser Valley using two Aerodyne aerosol mass spectrometers, Atmos. Environ., 38, 5745–5758, 2004.

Allan, J. D., Jimenez, J. L., Williams, P. I., Alfarra, M. R., Bower, K. N., Jayne, J. T., Coe, H., and Worsnop, D. R.: Quantitative sampling using an aerodyne aerosol mass spectrometer 1: Techniques of data interpretation and error analysis, J. Geophys. Res., 108, 4090, doi:10.1029/2002JD002358, 2003.

Allan, J. D., Delia, A. E., Coe, H., Bower, K. N., Alfarra, M. R., Jimenez, J. L., Middlebrook, A. M., Drewnick, F., Onasch, T. B., Canagaratna, M. R., Jayne, J. T., and Worsnop, D. R.: A generalized method for the extraction of chemically resolved mass spectra from Aerodyne Aerosol Mass Spectrometer data, J. Aerosol Sci., 35, 909–922, 2004.

Allan, J. D., Alfarra, M. R., Bower, K. N., Coe, H., Jayne, J. T., Worsnop, D. R., Aalto, P. P., Kulmala, M., Hyötyläinen, T., Cavalli, F., and Laaksonen, A.: Size and composition measurements of background aerosol and new particle growth in a Finnish forest during QUEST 2 using an Aerodyne Aerosol Mass Spectrometer, Atmos. Chem. Phys., 6, 315–327, doi:10.5194/acp-6-315-2006, 2006.

Andreae, M. O. and Rosenfeld, D.: Aerosol-cloud-precipitation interactions. Part 1. The nature and sources of cloud-active aerosols, Earth-Sci. Rev., 89, 13–41, 2008.

Asa-Awuku, A., Engelhart, G. J., Lee, B. H., Pandis, S. N., and Nenes, A.: Relating CCN activity, volatility, and droplet growth kinetics of β-caryophyllene secondary organic aerosol, Atmos. Chem. Phys., 9, 795–812, doi:10.5194/acp-9-795-2009, 2009.

Asa-Awuku, A., Nenes, A., Gao, S., Flagan, R. C., and Seinfeld, J. H.: Water-soluble SOA from Alkene ozonolysis: composition and droplet activation kinetics inferences from analysis of CCN activity, Atmos. Chem. Phys., 10, 1585–1597, doi:10.5194/acp-10-1585-2010, 2010.

Asa-Awuku, A., Moore, R. H., Nenes, A., Bahreini, R., Holloway, J. S., Brock, C. A., Middlebrook, A. M., Ryerson, T., Jimenez, J., DeCarlo, P., Hecobian, A., Weber, R., Stickel, R., Tanner, D. J., and Huey, L. G.: Airborne Cloud Condensation Nuclei Measurements during the 2006 Texas Air Quality Study, J. Geophys. Res., 116, D11201, doi:10.1029/2010JD014874, 2011.

Barth, M., McFadden, J. P., Sun, J., Wiedinmyer, C., Chuang, P., Collins, D., Griffin, R., Hannigan, M., Karl, T., Kim, S.-W., Lasher-Trapp, S., Levis, S., Litvak, M., Mahowald, N., Moore, K., Nandi, S., Nenes, A., Potosnak, M., Raymond, T. M., Smith,

J., Still, C., and Stroud, C.: Coupling between land ecosystems and the atmospheric hydrologic cycle through biogenic aerosol pathways, Bull. Amer. Meteor. Soc., 86, 1738–1742, 2005.

Birmili, W., Schwirn, K., Nowak, A., Petäjä, T., Joutsensaari, J., Rose, D., Wiedensohler, A., Hämeri, K., Aalto, P., Kulmala, M., and Boy, M.: Measurements of humidified particle number size distributions in a Finnish boreal forest: derivation of hygroscopic particle growth factors, Boreal Env. Res., 14, 458–480, 2009.

Bougiatioti, A., Fountoukis, C., Kalivitis, N., Pandis, S. N., Nenes, A., and Mihalopoulos, N.: Cloud condensation nuclei measurements in the marine boundary layer of the Eastern Mediterranean: CCN closure and droplet growth kinetics, Atmos. Chem. Phys., 9, 7053–7066, doi:10.5194/acp-9-7053-2009, 2009.

Bougiatioti, A., Nenes, A., Fountoukis, C., Kalivitis, N., Pandis, S. N., and Mihalopoulos, N.: Size-resolved CCN distributions and activation kinetics of aged continental and marine aerosol, Atmos. Chem. Phys., 11, 8791–8808, doi:10.5194/acp-11-8791-2011, 2011.

Boy, M., Petäjä, T., Dal Maso, M., Rannik, Ü., Rinne, J., Aalto, P., Laaksonen, A., Vaattovaara, P., Joutsensaari, J., Hoffmann, T., Warnke, J., Apostolaki, M., Stephanou, E. G., Tsapakis, M., Kouvarakis, A., Pio, C., Carvalho, A., Römpp, A., Moortgat, G., Spirig, C., Guenther, A., Greenberg, J., Ciccioli, P., and Kulmala, M.: Overview of the field measurement campaign in Hyytiälä, August 2001 in the framework of the EU project OSOA, Atmos. Chem. Phys., 4, 657–678, doi:10.5194/acp-4-657-2004, 2004.

Canagaratna, M. R., Jayne, J. T., Jimenez, J. L., Allan, J. D., Alfarra, M. R., Zhang, Q., Onasch, T. B., Drewnick, F., Coe, H., Middlebrook, A., Delia, A., Williams, L. R., Trimborn, A. M., Northway, M. J., DeCarlo, P. F., Kolb, C. E., Davidovits, P., and Worsnop, D. R.: Chemical and microphysical characterization of ambient aerosols with the Aerodyne aerosol mass spectrometer, Mass Spectrom. Rev., 26, 185–222, 2007.

Chang, R. Y.-W., Slowik, J. G., Shantz, N. C., Vlasenko, A., Liggio, J., Sjostedt, S. J., Leaitch, W. R., and Abbatt, J. P. D.: The hygroscopicity parameter (κ) of ambient organic aerosol at a field site subject to biogenic and anthropogenic influences: relationship to degree of aerosol oxidation, Atmos. Chem. Phys., 10, 5047–5064, doi:10.5194/acp-10-5047-2010, 2010.

Chuang, P. Y.: Measurements of the timescale of hygroscopic growth for atmospheric aerosols, J. Geophys. Res., 108, 4282, doi:10.1029/2002JD002757, 2003.

Chuang, P. Y., Charlson, R. J., and Seinfeld, J. H.: Kinetic limitations on droplet formation in clouds, Nature, 390, 594–596, 1997.

Crosier, J., Jimenez, J. L., Allan, J. D., Bower, K. N., Williams, P. I., Alfarra, M. R., Canagaratna, M. R., Jayne, J. T., Worsnop, D. R., and Coe, H.: Technical note: Description and use of the new Jump Mass Spectrum mode of operation for the Aerodyne Quadrupole Aerosol Mass Spectrometers (Q-AMS), Aerosol Sci. Technol., 41, 865–872, 2007.

Dusek, U., Frank, G. P., Curtius, J., Drewnick, F., Schneider, J., Kürten, A., Rose, D., Andreae, M. O., Borrmann, and Pöschl, U.: Enhanced organic mass fraction and decreased hygroscopicity of cloud condensation nuclei (CCN) during new particle formation events, Geophys. Res. Lett., 37, L03804, doi:10.1029/2009GL040930, 2010.

Ehn, M., Petäjä, T., Aufmhoff, H., Aalto, P., Hämeri, K., Arnold, F., Laaksonen, A., and Kulmala, M.: Hygroscopic properties of ultrafine aerosol particles in the boreal forest: diurnal variation, solubility and the influence of sulfuric acid, Atmos. Chem. Phys., 7, 211–222, doi:10.5194/acp-7-211-2007, 2007.

Engelhart, G. J., Asa-Awuku, A., Nenes, A., and Pandis, S. N.: CCN activity and droplet growth kinetics of fresh and aged monoterpene secondary organic aerosol, Atmos. Chem. Phys., 8, 3937–3949, doi:10.5194/acp-8-3937-2008, 2008.

Engelhart, G. J., Moore, R. H., Nenes, A., and Pandis, S. N.: Cloud condensation nuclei activity of isoprene secondary organic aerosol, J. Geophys. Res., 116, D02207, doi:10.1029/2010JD014706, 2011.

Good, N., Topping, D. O., Allan, J. D., Flynn, M., Fuentes, E., Irwin, M., Williams, P. I., Coe, H., and McFiggans, G.: Consistency between parameterisations of aerosol hygroscopicity and CCN activity during the RHaMBLe discovery cruise, Atmos. Chem. Phys., 10, 3189–3203, doi:10.5194/acp-10-3189-2010, 2010.

Gunn, R. and Woessner, R.: Measurements of the systematic electrification of aerosols, J. Coll. Sci., 11, 254–259, 1956.

Gunthe, S. S., King, S. M., Rose, D., Chen, Q., Roldin, P., Farmer, D. K., Jimenez, J. L., Artaxo, P., Andreae, M. O., Martin, S. T., and Pöschl, U.: Cloud condensation nuclei in pristine tropical rainforest air of Amazonia: size-resolved measurements and modeling of atmospheric aerosol composition and CCN activity, Atmos. Chem. Phys., 9, 7551–7575, doi:10.5194/acp-9-7551-2009, 2009.

Hämeri, K., Väkevä, M., Aalto, P. P., Kulmala, M., Swietlicki, E., Zhou, J., Seidl, W., Becker, E., and O'Dowd, C., D.: Hygroscopic and CCN properties of aerosol particles in boreal forests, Tellus, 53B, 359–379, 2001.

Hari, P. and Kulmala, M.: Station for Measuring Ecosystem–Atmosphere Relations (SMEAR II), Boreal Env. Res., 10, 315–322, 2005.

Intergovernmental Panel on Climate Change (IPCC), Climate Change 2007: The Physical Science Basis, Summary for Policymakers, http://www.ipcc.ch, 2007.

Irwin, M., Robinson, N., Allan, J. D., Coe, H., and McFiggans, G.: Size-resolved aerosol water uptake and cloud condensation nuclei measurements as measured above a Southeast Asian rainforest during OP3, Atmos. Chem. Phys. Discuss., 11, 3117–3159, doi:10.5194/acpd-11-3117-2011, 2011.

Jayne, J. T., Leard, D. C., Zhang, X., Davidovits, P., Smith, K. A., Kolb, C. E., Worsnop, D. R: Development of an aerosol mass spectrometer for size and composition analysis of submicron particles, Aerosol Sci. Technol., 33, 49–70, 2000.

Jensen, J. B. and Charlson, R. J.: On the efficiency of nucleation scavenging, Tellus, 36, 367–375, 1984.

Jimenez, J. L., Jayne, J. T., Shi, Q., Kolb, C. E., Worsnop, D. R., Yourshaw, I., Seinfeld, J. H., Flagan, R. C., Zhang, X., Smith, K. A., Morris, J., and Davidovits, P.: Ambient aerosol sampling using the Aerodyne Aerosol Mass Spectrometer, J. Geophys. Res., 108, 8425, doi:10.1029/2001JD001213, 2003.

Jimenez, J.L., Canagaratna, M. R., Donahue, N. M., Prevot, A. S. H., Zhang, Q., Kroll, J. H., DeCarlo, P. F., Allan, J. D., Coe, H., Ng, N. L., Aiken, A. C., Docherty, K. S., Ulbrich, I. M., Grieshop, A. P., Robinson, A. L., Duplissy, J., Smith, J. D., Wilson, K. R., Lanz, V. A., Hueglin, C., Sun, Y. L., Tian, J., Laaksonen, A., Raatikainen, T., Rautiainen, J., Vaattovaara, P., Ehn, M., Kulmala, M., Tomlinson, J. M., Collins, D. R., Cubison, M.

J., Dunlea, E. J., Huffman, J. A., Onasch, T. B., Alfarra, M. R., Williams, P. I., Bower, K., Kondo, Y., Schneider, J., Drewnick, F., Borrmann, S., Weimer, S., Demerjian, K., Salcedo, D., Cottrell, L., Griffin, R., Takami, A., Miyoshi, T., Hatakeyama, S., Shimono, A., Sun, J. Y., Zhang, Y. M., Dzepina, K., Kimmel, J. R., Sueper, D., Jayne, J. T., Herndon, S. C., Trimborn, A. M., Williams, L. R., Wood, E. C., Middlebrook, A. M., Kolb, C. E., Baltensperger, U., and Worsnop, D. R.: Evolution of organic aerosols in the atmosphere, Science, 326, 1525–1529, doi:10.1126/science.1180353, 2009.

Kanakidou, M., Seinfeld, J. H., Pandis, S. N., Barnes, I., Dentener, F. J., Facchini, M. C., Van Dingenen, R., Ervens, B., Nenes, A., Nielsen, C. J., Swietlicki, E., Putaud, J. P., Balkanski, Y., Fuzzi, S., Horth, J., Moortgat, G. K., Winterhalter, R., Myhre, C. E. L., Tsigaridis, K., Vignati, E., Stephanou, E. G., and Wilson, J.: Organic aerosol and global climate modelling: a review, Atmos. Chem. Phys., 5, 1053–1123, doi:10.5194/acp-5-1053-2005, 2005.

Köhler, H.: The nucleus in and the growth of hygroscopic droplets, T. Faraday Soc., 43, 1152–1161, 1936.

Kulmala, M., Laaksonen, A., Korhonen, P., Vesala, T., Ahonen, T., and Barrett, J. C.: The effect of atmospheric nitric acid vapour on CCN activation, J. Geophys. Res., 98, 22949–22958, 1993.

Kulmala, M., Hämeri, K., Aalto, P., Mäkelä, J.M., Pirjola, L., Nilsson, E. D., Buzorius, G., Rannik, Ü., Dal Maso, M., Seild, W., Hoffmann, T., Jansson, R., Hansson, H.-C., Viisanen, Y., Laaksonen, A. and O'Dowd, C. D.: Overview of the international project on biogenic aerosol formation in the boreal forest (BIOFOR), Tellus, 53B, 324–343, 2001.

Kulmala, M., Suni, T., Lehtinen, K. E. J., Dal Maso, M., Boy, M., Reissell, A., Rannik, Ü., Aalto, P., Keronen, P., Hakola, H., Bäck, J., Hoffmann, T., Vesala, T., and Hari, P.: A new feedback mechanism linking forests, aerosols, and climate, Atmos. Chem. Phys., 4, 557–562, doi:10.5194/acp-4-557-2004, 2004.

Kulmala, M., Asmi, A., Lappalainen, H. K., Carslaw, K. S., Pschl, U., Baltensperger, U., Hov, Ø., Brenquier, J.-L., Pandis, S. N., Facchini, M. C., Hansson, H.-C., Wiedensohler, A., and O'Dowd, C. D.: Introduction: European Integrated Project on Aerosol Cloud Climate and Air Quality interactions (EUCAARI) integrating aerosol research from nano to global scales, Atmos. Chem. Phys., 9, 2825–2841, doi:10.5194/acp-9-2825-2009, 2009.

Lance, S.: Quantifying compositional impacts of ambient aerosol on cloud droplet formation, Published Doctoral Thesis, available at: http://etd.gatech.edu/theses/available/etd-11132007-175217/unrestricted/lance_sara_m_200712_phd[1].pdf, 2007.

Lance, S., Nenes, A., and Rissman, T.: Chemical and dynamical effects on cloud droplet number: Implications for estimates of the aerosol indirect effect, J. Geophys. Res., 109, D22208, doi:10.1029/2004JD004596, 2004.

Lance, S., Medina, J., Smith, J. N., and Nenes, A.: Mapping the operation of the DMT continuous flow CCN counter, Aerosol Sci. Technol., 40, 242–254, 2006.

Lance, S., Nenes, A., Mazzoleni, C., Dubey, M. K., Gates, H., Varutbangkul, V., Rissmas, T. A., Murphy, S. M., Sorooshian, A., Flagan, R. C., Seinfeld, J. H., Feingold, G., and Jonsson, H. H.: Cloud condensation nuclei activity, closure, and droplet growth kinetics of Houston aerosol during the Gulf of Mexico Atmospheric Composition and Climate Study (GoMACCS), J. Geophys. Res., 114, D00F15, doi:10.1029/2008JD011699, 2009.

Lathem, T. L. and Nenes, A.: Water vapor depletion in the DMT Continuous Flow CCN Chamber: effects on supersaturation and droplet growth, Aerosol Sci. Technol., 45, 604–615, doi:10.1080/02786826.2010.551146, 2011.

Li, Z., Williams, A. L., and Rood, M. J.: Influence of Soluble Surfactant Properties on the Activation of Aerosol Particles Containing Inorganic Solute, J. Atmos. Sci., 55, 1859–1866, 1998.

Liu, B. Y. H., Pui, D. Y. H., Whitby, K. T., Kittelson, D. B., Kousaka, Y., and McKenzie, R. L.: The aerosol mobility chromatograph: A new detector for sulfuric acid aerosols, Atmos. Environ., 12, 99–104, 1978.

Massoli, P., Lambe, A. T., Ahern, A. T., Williams, L. R., Ehn, M., Mikkilä, Canagaratna, M. R., Brune, W. H., Onasch, T. B., Jayne, J. T., Petäjä, Kulmala, M., Laaksonen, A., Kolb, C. E., Davidovits, P., and Worsnop, D. R.: Relationship between aerosol oxidation level and hygroscopic properties of laboratory generated secondary organic aerosol (SOA) particles, Geophys. Res. Lett., 37, L24801, doi:10.1029/2010GL045258, 2010.

Medina, J., Nenes, A., Sotiropoulou, R.-E. P., Cotrell, L. D., Ziembia, L. D., Beckman, P. J., and Griffin, R. J.: Cloud condensation nuclei closure during the International Consortium for Atmospheric Research on Transport and Transformation 2004 campaign: Effects of size-resolved composition, J. Geophys. Res., 112, D10S31, doi:10.1029/2006JD007588, 2007.

Mochida, M., Nishita-Hara, C., Kitamori, Y., Aggarwal, S. G., Kawamura, K., Miura, K., and Takami, A.: Size-segregated measurements of cloud condensation nucleus activity and hygroscopic growth for aerosols at Cape Hedo, Japan, in spring 2008, J. Geophys. Res., 115, D21207, doi:10.1029/2009JD013216, 2010.

Moore, R., Nenes, A., and Medina, J.: Scanning Mobility CCN Analysis – A method for fast measurements of size resolved CCN distributions and activation kinetics, Aerosol Sci. Technol., 44, 861–871, 2010.

Murphy, S. M., Agrawal, H., Sorooshian, A., Padro, L. T., Gates, H., Hersey, S., Welch, W. A., Jung, H., Miller, J. W., Cocker, D.R., Nenes, A., Jonsson, H., Flagan, R. C., and Seinfeld, J. H.: Comprehensive simultaneous shipboard and airborne characterization of exhaust from a modern container ship at sea, Environ. Sci. Technol., 43, 4626–4640, 2009.

Nemitz, E., Jimenez, J. L., Huffman, J. A., Ulbrich, I. M., Canagaratna, M. R., Worsnop, D. R., and Guenther, A. B.: An eddy-covariance system for the measurement of surface/atmosphere exchange fluxes of submicron aerosol chemical species – first application above an urban area, Aerosol Sci. Technol., 42, 636–657, 2008.

Nenes, A., Ghan, S., Abdul-Razzak, H., Chuang, P. Y., Seinfeld, J. H.: Kinetic limitations on cloud droplet formation and impact on cloud albedo, Tellus, 53B, 133–149, 2001.

Nenes, A., Charlson, R. J., Facchini, M. C., Kulmala, M., Laaksonen, A., and Seinfeld, J. H.: Can chemical effects on cloud droplet number rival the first indirect effect?, Geophys. Res. Lett., 29, 1848, doi:10.1029/2002GL015295, 2002.

Nieminen, T., Manninen, H. E., Sihto, S.-L., Yli-Juuti, T., Mauldin III, R. L., Petäjä, T., Riipinen, I., Kerminen, V.-M., and Kulmala, M.: Connection of sulfuric acid to atmospheric nucleation in boreal forest, Environ. Sci. Technol., 43, 4715–4721, 2009.

Padró, L. T., Asa-Awuku, A., Morrison, R., and Nenes, A.: Inferring thermodynamic properties from CCN activation experiments: single-component and binary aerosols, Atmos. Chem. Phys., 7, 5263–5274, doi:10.5194/acp-7-5263-2007, 2007.

Padró, L. T., Tkacik, D., Lathem, T., Hennigan, C., Sullivan, A.P., Weber, R.J., Huey, L.G., and Nenes, A.: Investigation of cloud condensation nuclei properties and droplet growth kinetics of the water-soluble aerosol fraction in Mexico City, J. Geophys. Res., 115, D09204, doi:10.1029/2009JD013195, 2010.

Petäjä, T., Kerminen, V.-M., Hämeri, K., Vaattovaara, P., Joutsensaari, J., Junkermann, W., Laaksonen, A., and Kulmala, M.: Effects of SO_2 oxidation on ambient aerosol growth in water and ethanol vapours, Atmos. Chem. Phys., 5, 767–779, doi:10.5194/acp-5-767-2005, 2005.

Petters, M. D and Kreidenweis, S. M.: A single parameter representation of hygroscopic growth and cloud condensation nucleus activity, Atmos. Chem. Phys., 7, 1961–1971, 2007, http://www.atmos-chem-phys.net/7/1961/2007/.

Petters, M. D., Carrico, C. M., Kreidenweis, S. M., Prenni, A. J., DeMott, P. J., Collett Jr., J. L., and Moosmüller, H.: Cloud condensation nucleation activity of biomass burning aerosol, J. Geophys. Res., 114, D22205, doi:10.1029/2009JD012353, 2009.

Pöschl, U.: Gas-particle interactions of tropospheric aerosols: Kinetic and thermodynamic perspectives of multiphase chemical reactions, amorphous organic substances, and the activation of cloud condensation nuclei, Atmos. Res., 101, 562–573, doi:10.1016/j.atmosres.2010.12.018, 2011.

Pöschl, U., Martin, S. T., Sinha, B., Chen, Q., Gunthe, S. S., Huffman, J. A., Borrmann, S., Farmer, D. K., Garland, R. M., Helas, G., Jimenez, J. L., King, S. M., Manzi, A., Mikhailov, E., Pauliquevis, T., Petters, M. D., Prenni, A. J., Roldin, P., Rose, D., Schneider, J., Su, H., Zorn, S. R., Artaxo, P., and Andreae, M. O.: Rainforest aerosols as biogenic nuclei of cloud and precipitation in the Amazon, Science, 329, 1513–1516, doi:10.1126/science.1191056, 2010.

Prenni, A. J., Petters, M. D., Kreidenweis, S. M., DeMott, P. J., and Ziemann, P. J.: Cloud droplet activation of secondary organic aerosol, J. Geophys. Res., 112, D10223, doi:10.1029/2006JD007963, 2007.

Pringle, K. J., Tost, H., Pozzer, A., Pöschl, U., and Lelieveld, J.: Global distribution of the effective aerosol hygroscopicity parameter for CCN activation, Atmos. Chem. Phys. Discuss., 10, 6301–6339, doi:10.5194/acpd-10-6301-2010, 2010.

Raatikainen, T., Vaattovaara, P., Tiitta, P., Miettinen, P., Rautiainen, J., M. Ehn, M., Kulmala, M., Laaksonen, A., and Worsnop, D. R.: Physicochemical properties and origin of organic groups detected in boreal forest using an aerosol mass spectrometer, Atmos. Chem. Phys., 10, 2063–2077, 2010, http://www.atmos-chem-phys.net/10/2063/2010/.

Rader, D. J. and McMurry, P. H.: Application of the tandem differential mobility analyzer to studies of droplet growth or evaporation, J. Aerosol Sci., 17, 771–787, 1986.

Raymond, T. and Pandis, S. N.: Cloud activation of single-component organic aerosol particles, J. Geophys. Res., 107, 4787, doi:10.1029/2002JD002159, 2002.

Roberts, G. and Nenes, A.: A Continuous-Flow Streamwise Thermal-Gradient CCN Chamber for atmospheric measurements, Aerosol Sci. Technol., 39, 206–221, 2005.

Rose, D., Gunthe, S. S., Mikhailov, E., Frank, G. P., Dusek, U., Andreae, M. O., and Pöschl, U.: Calibration and measurement uncertainties of a continuous-flow cloud condensation nuclei counter (DMT-CCNC): CCN activation of ammonium sulfate and sodium chloride aerosol particles in theory and experiment, Atmos. Chem. Phys., 8, 1153–1179, doi:10.5194/acp-8-1153-2008, 2008.

Rose, D., Nowak, A., Achtert, P., Wiedensohler, A., Hu, M., Shao, M., Zhang, Y., Andreae, M. O., and Pöschl, U.: Cloud condensation nuclei in polluted air and biomass burning smoke near the mega-city Guangzhou, China - Part 1: Size-resolved measurements and implications for the modeling of aerosol particle hygroscopicity and CCN activity, Atmos. Chem. Phys., 10, 3365–3383, doi:10.5194/acp-10-3365-2010, 2010.

Ruehl, C. R., Chuang, P. Y., and Nenes, A.: How quickly do cloud droplets form on atmospheric particles?, Atmos. Chem. Phys., 8, 1043–1055, doi:10.5194/acp-8-1043-2008, 2008.

Ruehl, C. R., Chuang, P. Y. and Nenes, A.: Distinct CCN activation kinetics above the marine boundary layer along the California coast, Geophys. Res. Let., 36, L15814, doi:10.1029/2009GL038839, 2009.

Seinfeld, J. H. and Pandis, S. N.: Atmospheric Chemistry and Physics: From Air Pollution to Climate Change, 2, John Wiley & Sons, Inc., Hoboken, NJ, 2006.

Shulman, M. L., Jacobson, M. C., Carlson, R. J., Synovec, R. E., and Young, T. E.: Dissolution behavior and surface tension effects of organic compounds in nucleating cloud droplets, Geophys. Res. Let, 23, 277–280, doi:10.1029/95GL03810, 1996.

Sihto, S.-L., Mikkilä, J., Vanhanen, J., Ehn, M., Liao, L., Lehtipalo, K., Aalto, P. P., Duplissy, J., Petäjä, T., Kerminen, V.-M., Boy, M., and Kulmala, M.: Seasonal variation of CCN concentrations and aerosol activation properties in boreal forest, Atmos. Chem. Phys. Discuss., 10, 28231-28272, doi:10.5194/acpd-10-28231-2010, 2010.

Sorooshian, A., Murphy, S. M., Hersey, S., Gates, H., Padro, L. T., Nenes, A., Brechtel, F. J., Jonsson, H., Flagan, R. C., and Seinfeld, J. H.: Comprehensive airborne characterization of aerosol from a major bovine source, Atmos. Chem. Phys. Discuss., 8, 10415–10479, doi:10.5194/acpd-8-10415-2008, 2008.

Su, H., Rose, D., Cheng, Y. F., Gunthe, S. S., Massling, A., Stock, M., Wiedensohler, A., Andreae, M. O., and Pöschl, U.: Hygroscopicity distribution concept for measurement data analysis and modeling of aerosol particle mixing state with regard to hygroscopic growth and CCN activation, Atmos. Chem. Phys., 10, 7489–7503, doi:10.5194/acp-10-7489-2010, 2010.

Swietlicki, E., Hansson, H.-C., Hämeri, K., Svenningsson, B., Massling, A., McFiggans, G., McMurry, P.H., Petäjä, T., Tunved, P., Gysel, M., Topping, D., Weingartner, E., Baltensperger, U., Rissler, J., Wiedensohler, A. and Kulmala, M.: Hygroscopic properties of sub-micrometer atmospheric aerosol particles measured with H-TDMA instruments in various environments – a review, Tellus, 60B, 432–469, 2008.

Twomey, S.: Pollution and the planetary albedo, Atmos. Environ., 8, 1251–1256, 1974.

Twomey, S.: The influence of pollution on the shortwave albedo of clouds, J. Atmos. Sci., 34, 1149–1152, 1977.

Väkevä, M., Kulmala, M., Stratmann, F., and Hämeri, K.: Field measurements of hygroscopic properties and state of mixing of nucleation mode particles, Atmos. Chem. Phys., 2, 55–66, doi:10.5194/acp-2-55-2002, 2002.

Wang, S. C. and Flagan, R. C.: Scanning Electrical Mobility Spectrometer, Aerosol Sci. Technol., 13, 230–240, 1990.

Wiedensohler, A. and Fissan, H. J.: Aerosol charging in high purity gases, J. Aerosol Sci., 19, 867–870, 1988.